Second-order Born collisional stopping of ions in a free-electron gas

D. G. Arbó, M. S. Gravielle, and J. E. Miraglia*
Instituto de Astronomía y Física del Espacio, Consejo Nacional de Investigaciones Científicas y Técnicas, Casilla de Correos 67, Sucursal 28, 1428 Buenos Aires, Argentina
and Departamento de Física, FCEyN, Universidad de Buenos Aires, Buenos Aires, Argentina
(Received 12 April 2000; published 17 August 2000)

The energy loss of a heavy bare projectile with charge Z_P moving in a free-electron gas is studied within the framework of the binary collisional formalism. The transition-matrix element is expanded in a perturbative series, and terms up to Z_P^3 (second Born approximation) are conserved. The Mermin-Lindhard dielectric response function is employed to describe the cylindric potential induced by the projectile. The formalism is applied to the calculation of energy-loss distributions for fixed charges (protons, neutral hydrogen, and antiprotons) colliding with aluminum. We also investigate how the Z_P^3 collisional correction affects the total stopping for antiprotons in aluminum and silicon, and for protons in aluminum. In this latest case, different charge states of the projectile are considered. Results are in good agreement with experimental data in the high-energy region.

PACS number(s): 34.50.Bw, 34.50.Dy, 34.50.Fa, 79.20.Rf

I. PRELIMINARY

In a previous paper [1], we calculated the first perturbative order of the stopping power for a fast ion moving through a free-electron gas (FEG). We worked within the framework of the binary collisional formalism (BCF), also called kinetic theory [2]. This formalism is based on the assumption that *individual* electrons (e) are scattered by the projectile (P), with charge Z_P, moving inside the solid. As these two particles are within a FEG, the Coulomb P-e interaction is shielded by the presence of the other electrons which react to the presence of a moving projectile, creating a so-called wake potential. The first perturbative order of the stopping power depends on Z_P^2, being therefore insensitive to the sign of projectile charge, i.e., protons and antiprotons give the same results.

In the present work, we go further and calculate the second perturbative order of the transition-matrix element. By introducing this element in the BCF, the Z_P^3 collisional correction to the stopping power is obtained. As in I, the shielded P-e potential is calculated in terms of the Mermin-Linhard dielectric response function, which leads to a full cylindric potential. The Z_P^3 collisional contribution to both the differential energy-loss distribution and the stopping is examined and discussed in terms of the sign of the projectile charge and the impact velocity. Present calculations differ from previous ones in the fact that a proper *cylindric*-induced potential is employed here instead of a *spherically* symmetric one [3–5].

With the aim of studying how the Z_P^3 collisional correction affects the total energy loss, we calculate the total stopping power. It is obtained by adding to the first-order stopping in the dielectric formalism, the second-order contributions due to binary collisions not only with the free-electron gas but also with electrons belonging to atomic inner shells. The stopping originated by inner-shell ionization is evaluated with the continuum distorted wave–eikonal initial state (CDW-EIS) approximation [6,7], which includes all orders in Z_P, at least approximately. Our results are compared with experimental data for antiprotons in aluminum and silicon and for protons in aluminum. In the case of incident protons, we take into account the projectile structure by weighting the stopping of the different exiting products with the equilibrium charge state fractions [8].

The work is organized as follows. In Sec. II we present the theory, in Sec. III the results, and in Sec. IV the conclusions are summarized. We here employ the same notation as Ref. [1]. Atomic units are used except where indicated.

II. THEORY

Let us consider a heavy projectile P moving with velocity v within a solid and losing energy by binary collisions with electrons of the FEG. Schematically, we deal with the following two-particle (P-e) process

$$P^{Z_P+}_{\vec{K}_i} + e^{-}_{\vec{k}_i} \rightarrow P^{Z_P+}_{\vec{K}_f} + e^{-}_{\vec{k}_f}, \tag{1}$$

where $\vec{K}_i,(\vec{K}_f),\vec{k}_i(\vec{k}_f)$ are the initial (final) projectile and electron momenta, respectively. The Fermi golden rule states that the sevenfold differential probability per unit length and per unit of lost energy $d\omega$ for the electronic transition $\vec{k}_i \rightarrow \vec{k}_f$ is given by

$$\frac{d^7W}{d\omega d\vec{k}_i d\vec{k}_f} = \frac{2\pi}{v}\,\delta\left(\frac{k_i^2}{2} - \frac{k_f^2}{2} + \omega\right)\delta(\omega - \vec{v}\cdot\vec{q})|T|^2, \tag{2}$$

where $T = \langle \psi_{\vec{k}_f} | V_{Pe} | \Psi^{+}_{\vec{k}_i} \rangle$ is the transition-matrix element, V_{Pe} is the P-e potential, $\psi_{\vec{k}_f}$ is the unperturbed final state, and $\Psi^{+}_{\vec{k}_i}$ is the exact outgoing scattering state. In Eq. (2) $\vec{q}$ ($\vec{p}$) is the electron (projectile) momentum transfer; $\vec{q} = \vec{K}_i$

*Also at Universidad Nacional de La Matanza, Argentina.

$-\vec{K}_f=\vec{k}_f-\vec{k}_i=-\vec{p}$, and with this definition the lost energy $\omega=\vec{q}\cdot\vec{v}$ is positive. The wake potential V_{Pe} describes the Coulomb P-e interaction shielded by the other electrons of the solid, which react to the presence of a moving charge. This potential is here evaluated in terms of the Mermin-Linhard dielectric response function of the FEG, $\epsilon(q,\omega)$ [see Eq. (5)]. In the derivation of Eq. (2), the projectile mass is considered infinity.

As usual in atomic collisions theory, the T matrix can be expanded in a perturbative series by using undistorted plane-wave states $\psi_{\vec{k}_{i,f}}$ to describe the electronic continuum state, thus it yields the well-known Born series, $T=\Sigma_j T_j$. Conserving up to third order in the projectile charge, we can write

$$|T|^2=|T_1+T_2|^2=|T_1|^2+2\mathrm{Re}[T_1T_2^*]+\mathcal{O}(Z_P^4), \tag{3}$$

being the first and second term on the right-hand side proportional to Z_P^2 and Z_P^3, respectively. Replacing Eq. (3) in Eq. (2) the stopping power is obtained by integration, after multiplying by the energy loss ω, to give

$$S^{BC}=\int d\vec{k}_i\, d\vec{k}_f\, d\omega\ \omega\ \Theta(k_F-k_i)\Theta(k_f-k_F) \times\left(\frac{d^7W}{d\omega d\vec{k}_i d\vec{k}_f}\right)=S_1^{BC}+S_2^{BC}, \tag{4}$$

where S_1^{BC} and S_2^{BC} are proportional to Z_P^2 and Z_P^3, respectively. Terms of order Z_P^4 were neglected in Eq. (4). The superindex BC denotes that the stopping corresponds to the binary collisional mechanism. The two Heaviside step functions Θ in Eq. (4) refer to the $T=0$ K Fermi distribution and the Pauli exclusion principle (k_F is the Fermi momentum). In Secs. II A and II B we resume the first and second Born approximation, respectively, within the BCF.

A. The first Born approximation

The first order of the transition-matrix element is simply the Fourier transform of the potential P-e, i.e., $T_1=(2\pi)^{-3/2}\tilde{V}_{Pe}(\vec{q})$, $\tilde{V}_{Pe}(\vec{q})=-Z_P\tilde{V}_\epsilon(\vec{q})$, where

$$\tilde{V}_\epsilon(\vec{q})=f(q)\frac{1}{\epsilon(q,\omega,\gamma)}\sqrt{\frac{2}{\pi}}\frac{1}{q^2}, \tag{5}$$

and $\epsilon(q,\omega,\gamma)$ is the dielectric function of the FEG. The function $f(q)$ is included in Eq. (5) to account for the distribution of the electronic cloud in the case of dressed projectiles (see Sec. II C). For bare projectiles $f(q)=1$. Along this work the function $\epsilon(q,\omega,\gamma)$ is calculated by employing the Mermin prescription, which extends the Lindhard's dielectric function $\epsilon_L(q,\omega,0^+)$ to the finite lifetime $1/\gamma$ [9,10].

As it was shown in Ref. [1], the first-order stopping in the BCF reads

$$S_1^{BC}=-\frac{2Z_P^2}{\pi v^2}\int_0^\infty\frac{dq}{q}f^2(q)\int_0^{qv}d\omega\ \omega\ \mathrm{Im}\left[\frac{1}{\epsilon(q,\omega,\gamma)}\right] \times U_\epsilon(q,\omega,\gamma)=\mathcal{F}(U_\epsilon), \tag{6}$$

where

$$U_\epsilon(q,\omega,\gamma)=\frac{\mathrm{Im}\epsilon_L(q,\omega,0^+)}{\mathrm{Im}\epsilon(q,\omega,\gamma)}\to U_L(q,\omega)=\Theta(k_F^2-B^2), \tag{7}$$

as $\gamma\to 0$ with $B=(\omega-q^2/2)/q$.

The link between the BCF and the dielectric formalism (DF) can be detected straightforwardly from Eq. (6). In the DF the stopping reads simply as $S_1^{DF}=\mathcal{F}(U_\epsilon=1)$ [11], while the BCF requires, as observed in Eq. (6), $S_1^{BC}=\mathcal{F}(U_\epsilon(q,\omega,\gamma))$. The stopping power in the DF includes not only the binary mechanism in the first Born approximation but also the collective response.

B. The second Born approximation

In the Born approximation, the second order of the transition matrix reads

$$T_2=\langle\psi_{\vec{k}_f}|V_{Pe}(\vec{r})G_0^+V_{Pe}(\vec{r})|\psi_{\vec{k}_i}\rangle =\frac{1}{(2\pi)^6}\int d\vec{k}\tilde{V}_{Pe}(\vec{k})\tilde{V}_{Pe}(\vec{q}-\vec{k}) \times\left[E-\frac{1}{2}(\vec{k}_i-\vec{k})^2+i\eta\right]^{-1}, \tag{8}$$

where $G_0^+=(E-H_0+i\eta)^{-1}$ is the retarded Green function (the limit $\eta\to 0^+$ must be understood), E is the total energy, and H_0 is the kinetic energy operator. Note that this second order corresponds to a *cylindric* potential. If a *spherical* potential had been used instead, the exact transition amplitude could have been obtained with the usual partial wave expansion [3,4]. Since we are not interested here in electronic distributions [12], we can transform $d\vec{k}_i d\vec{k}_f\to d\vec{k}_i d\vec{q}$ in Eq. (2) making much easier the calculations to come. Replacing T_1 and T_2 in Eq. (3), and this one in Eqs. (2) and (4), we can exchange the integrations on $\vec{k}$ and $\vec{q}$, and after much algebra we find

$$S_2^{BC}=\frac{-2Z_P^3}{\pi v^2}\int_0^\infty\frac{dq}{q}f(q)\int_0^\infty d\omega\frac{\omega}{|\epsilon(q,\omega,\gamma)|^2} \times\mathrm{Re}[\epsilon(q,\omega,\gamma)A_1(\vec{q},v)], \tag{9}$$

where

$$A_1(\vec{q},v)=\frac{1}{2\pi^2}\int d\vec{k}\ \tilde{V}_\epsilon(\vec{k})P(\vec{q},\vec{k},v)\tilde{V}_\epsilon(\vec{q}-\vec{k}) \tag{10}$$

and

$$P(\vec{q},\vec{k},v)=\int d\vec{k}_i\ \Theta(k_F-k_i)\Theta(|\vec{q}-\vec{k}_i|-k_F)$$
$$\times\frac{\delta\left[\vec{q}\cdot\vec{v}-\left(\vec{q}\cdot\vec{k}_i+\frac{1}{2}q^2\right)\right]}{\left(-\frac{k^2}{2}-\vec{v}\cdot\vec{k}+\vec{k}_i\cdot\vec{k}+i\eta\right)}. \quad (11)$$

Note that A_1 has the same structure as the second Born T-matrix element T_2, but now $P(\vec{q},\vec{k},v)$, instead of G_0^+, represents a propagator which takes account of the convolution on the Fermi sphere. The integral in Eq. (11) can be evaluated analytically, giving

$$P(\vec{q},\vec{k},v)=\frac{\mathrm{sgn}(R_1)}{qk^2\sin^2\theta}R_2U_L(q,\omega), \quad (12)$$

where

$$R_1=k_zB-\frac{k^2}{2}-\vec{v}\cdot\vec{k},\quad R_2=\sqrt{u(k_m)}-\sqrt{u(k_F)}, \quad (13)$$

$$u(k_x)=\{(R_1+i\eta)^2-k^2(k_x^2-B^2)\sin^2\theta\}, \quad (14)$$

$$k_m=\begin{cases}|B| & \text{if } k_F^2-2\omega\leqslant 0\\ \max(k_{m1},k_{m2}) & \text{if } k_F^2-2\omega>0,\end{cases} \quad (15)$$

$$k_{m1}=\sqrt{k_F^2-2\omega},\quad k_{m2}=|B|, \quad (16)$$

$\cos\theta=\hat{q}\cdot\hat{k}$, $k_z=\vec{k}\cdot\hat{q}$, $\hat{q}=\vec{q}/q$, $\hat{k}=\vec{k}/k$, and B was defined below Eq. (7). In Eq. (12) the function $U_L(q,\omega)=\Theta(k_F-k_m)$ defines the binary region, as given by Eq. (7).

It is interesting to note that in the BC formalism the second Born approximation of stopping power writes in similar fashion to the first order given by Eq. (6), if a second-order dielectric function, including only the collisional correction, is considered, i.e.,

$$S^{BC}=S_1^{BC}+S_2^{BC}=-\frac{2Z_P^2}{\pi v^2}\int_0^\infty\frac{dq}{q}f(q)\int_0^{qv}d\omega\ \omega$$
$$\times\mathrm{Im}\left[\frac{f(q)+iZ_PA_1^*}{\epsilon_L(q,\omega,0^+)}\right]U_L(q,\omega). \quad (17)$$

Although this expression was derived only for the Lindhard dielectric constant, we have extended to other dielectric functions such as the Mermin-Lindhard dielectric function. Equation (17) shows directly the correction up to Z_P^3 order to the stopping power as far as a binary collision is concerned.

C. Stopping of dressed projectiles

The preceding equations are fulfilled for the case of bare projectiles considering $f(q)=1$. This is not the case of dressed projectiles. We consider here that the projectile electrons do not suffer transitions, remaining unperturbed during the collision. In this frozen approximation, for projectiles containing one or two electrons in the ground state, the binary collisions with the FEG can be described by approximating in the potential V_{Pe} the function $f(q)$ by $f(q)=1-F(q)/Z_P$. $F(q)$ is the well-known atomic form factor which can be approximated by

$$F(q)=\sum_{n=1}^{n_p}\frac{(2z_n)^4}{(4z_n^2+q^2)^2}, \quad (18)$$

n_p is the number of electrons in the $1s$ ground state, and z_n the effective charges seen by each projectile electron [15] (see Refs. [13,14] for the case of incident He^+). In the calculations, for incident $H^0(n_p=1)$ we consider $z_n=1$.

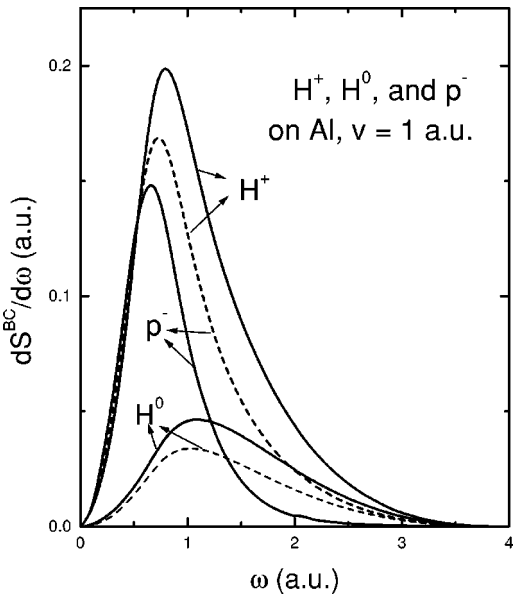

FIG. 1. Energy-loss distributions for 25 keV ($v=1$ a.u.) protons, antiprotons, and neutral hydrogen on aluminum solid targets considering fixed-charge projectile. Solid lines, the second-order contributions $dS^{BC}/d\omega=dS_1^{BC}/d\omega+dS_2^{BC}/d\omega$; dashed lines, the first-order contributions $dS_1^{BC}/d\omega$.

III. RESULTS

We study two different solid targets, aluminum and silicon. The parameters used to describe them are the following. For aluminum, the electron density of the FEG is $N_e=0.0268$ a.u. (or equivalently, the plasmon frequency $\omega_p=0.58$ a.u., and Fermi momentum $k_F=0.927$ a.u.), the atomic density $N_{at}=8.92\times10^{-3}$ a.u., and $\gamma=0.037$ a.u. [16]. For silicon, $N_e=0.0296$ a.u. ($\omega_p=0.61$ a.u., $k_F=0.957$ a.u.), $N_{at}=7.4\times10^{-3}$ a.u., and $\gamma=0.156$ a.u. [17]. Calculations of the Z_P^3- collisional correction S_2^{BC} involve a five-dimensional numerical integration: three on $\vec{k}$ as given in Eq. (10), and two additional integrations on q and ω as shown in Eq. (9).

In Fig. 1 we display the contribution of the binary collisions with a FEG to energy-loss distribution, $dS^{BC}/d\omega$, for neutral and single-charged projectiles moving inside an aluminum target. Three projectiles with fixed charges are con-

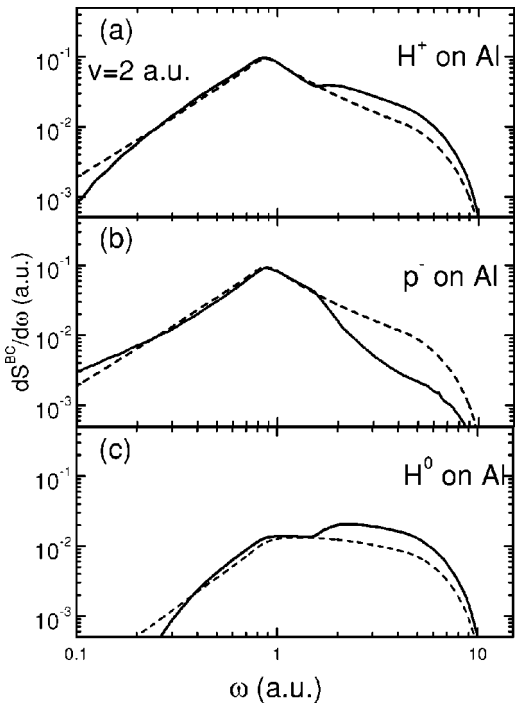

FIG. 2. Energy-loss distributions for 100 keV ($v=2$ a.u.) protons, antiprotons, and neutral hydrogen on aluminum solid targets considering the projectile charge as fixed. Solid lines, the second-order contributions $dS^{BC}/d\omega = dS_1^{BC}/d\omega + dS_2^{BC}/d\omega$; dashed lines, the first-order contributions $dS_1^{BC}/d\omega$.

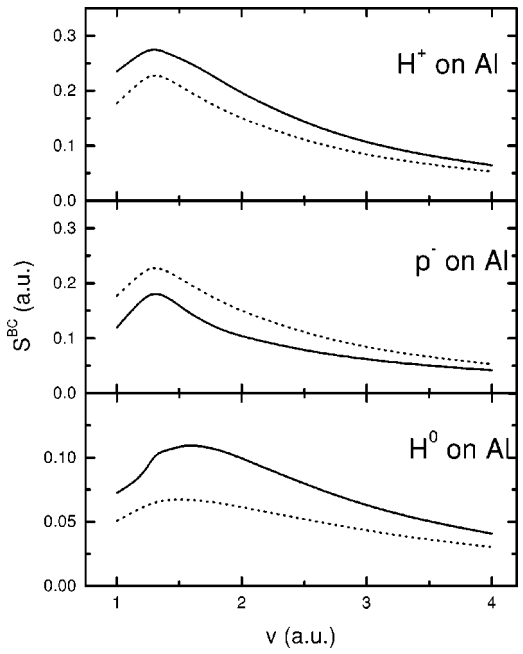

FIG. 3. Stopping power for protons, antiprotons, and neutral hydrogen on aluminum solid targets as a function of the impact velocity, considering the projectile charge as fixed. Solid lines, second-order collisional stopping $S^{BC}=S_1^{BC}+S_2^{BC}$; the dashed lines correspond to the first-order S_1^{BC}.

sidered, i.e., H^+, $\overline{p}$, and H^0. The incident velocity $v=1$ a.u. (25 keV) represents the lowest velocity that can be considered with our perturbative model, which is valid for $v > k_F$. Note that at this impact energy, both inner shell and collective contributions are negligible, allowing us to scrutinize in detail the behavior of the stopping due to binary collisions with the FEG. We also show in Fig. 1 the first Born collisional contribution $dS_1^{BC}/d\omega$, which averages results for H^+ and $\overline{p}$. As is mentioned above, the collisional contribution $dS_2^{BC}/d\omega$ is strictly proportional to Z_P^3, showing the same absolute value for projectile charges with opposite signs. For protons, $dS_2^{BC}/d\omega > 0$ in all the energy-loss range, indicating that protons deposit more energy in the solid than the first-order prediction. On the other hand, for antiprotons impact $dS_2^{BC}/d\omega < 0$. For H^0 projectiles, the contribution of the second order $dS_2^{BC}/d\omega$ is positive, as in the case of protons.

Figure 2 shows collisional binary contribution to energy-loss distribution, $dS^{BC}/d\omega$, for 100 keV ($v=2$ a.u.) protons [Fig. 2(a)], antiprotons [Fig. 2(b)], and neutral hydrogen [Fig. 2(c)] moving in aluminum. Figure 2(a) shows that for incident protons the second Born contribution reinforces a significant portion of the binary contribution to the stopping at high values of ω ($\omega > 1$ a.u.). Conversely, as shown in Fig. 2(b) for antiprotons it is canceled by the second-order term for $\omega > 1$ a.u. In other words, antiprotons seem to partially avoid head-on collisions with the FEG, which involve high energy transferred, while they are strengthened for the proton impact. The contribution $dS^{BC}/d\omega$ for neutral hydrogen [Fig. 2(c)] has the same qualitative shape as protons for $\omega > 1$. As was shown in I at high velocities and for large ω, the influence of structure of the projectile in the stopping is not relevant since the collisions take place very close to the impinging nucleus.

The total binary contribution to the stopping, S^{BC}, as given in Eq. (4), is plotted in Fig. 3 for H^+, $\overline{p}$, and H^0 impinging on aluminum as a function of the projectile velocity. In the three cases the projectile charge is considered fixed. The stopping of H^0 is substantially smaller than the ones corresponding to H^+ and $\overline{p}$ (note that different scales are used). The first-order predictions for protons and antiprotons are obviously the same because they depend on Z_P^2. In the whole velocity range considered, the Z_P^3 collisional correction S_2^{BC} increases the binary stopping for protons, and lowers it for antiprotons, in the same (symmetric) amount with respect to the first-order contribution S_1^{BC}. In both cases, when the velocity increases the contribution S_2^{BC} vanishes. For incident H^0 the second-order contribution S_2^{BC} is of the same order as that of protons, while stopping corresponding to the first Born approximation is approximately a factor 2 smaller than the first order for protons, at the lowest velocities considered.

To investigate in detail to what extent the Z_P^3 collisional correction affects the total stopping power, we need to take into account other contributions, such as inner-shell collisions and capture and loss processes, while for the case of antiprotons, these latest processes do not exist; for incident protons its contribution is estimated as less than 10%, being then neglected in the present work. The inner-shell contribu-

tion remains in both cases, protons and antiprotons, and it is originated by ionization of the target atoms as consequence of binary collisions with the projectile. It is calculated by using the CDW-EIS theory [6,7], which includes all orders on Z_P, at least approximately. This approximation has proved to successfully explain atomic ionization processes in a large variety of collisional systems, see for example [18]. In this work the initial bound states are described by Hartree-Fock Clementi-Roetti double-Z functions [19], while a Coulomb wave function with a charge satisfying the binding energy is employed to describe the final continuum state.

We studied in detail the ionization of the L shell for the case H^+ on Al. Several uncertainties were found in relation to the parameters to be used, as it is resumed next. For $v=3$, the energy loss due to ionization of the L shell of a neutral atom (namely Al^0) calculated with the CDW-EIS yields 7.03 a.u., i.e., 55% above the value 4.55 a.u. obtained by Oddershede and Sabin [20]. A first correction to be considered is that not all the final electron states in the continuum are possible. Due to the Pauli principle the range of final electron states with $k_f \in \{0,k_F\}$ is forbidden, since such final states are already occupied by the FEG. By dropping the contribution of these banned states the energy loss reduces slightly from 7.03 to 6.54 a.u. Then, an uncertainty arises: to what extent should we consider the initial atomic orbital as described by Al^0 and not by Al^{3+}? The latter is more realistic since the three outer electrons were ceded to the FEG. For the case of protons colliding on Al^{3+}, the CDW-EIS considerably reduces its value, from 6.54 to 4.85 a.u., which now is very near the value 4.55 a.u. obtained by Oddershede and Sabin [20]. Therefore, to describe the target bound states we employ Table 17 of Ref. [19] corresponding to ions Al^{3+} and Si^{4+}. In both cases only ionization from the L shell is considered.

For a fixed charge of the projectile, we calculate the total stopping S by adding to the first-order stopping by collisions with the FEG S_1^{DF}, the Z_P^3 collisional correction S_2^{BC}, and the inner-shell contribution $S_{CDW\text{-}EIS}^{IS}$, which includes Z_P^3 and higher corrections, at least approximately, i.e.,

$$S = S_1^{DF} + S_2^{BC} + S_{CDW\text{-}EIS}^{IS}. \tag{19}$$

As mentioned above, the first-order stopping in the DF, S_1^{DF}, corresponds to the sum of binary and collective contributions, being proportional to Z_P^2. Therefore, the total stopping S contains second-order corrections originated from binary collisions with both free-electron gas and core electrons, while collective effects are only considered in first perturbative order. Higher orders of the collective contribution are expected to be important at the lower velocities studied.

As a reference we also calculate the first-order total stopping S_1, which is obtained as a sum of S_1^{DF} and the first-order inner-shell stopping S_{Born}^{IS}, i.e.,

$$S_1 = S_1^{DF} + S_{Born}^{IS}. \tag{20}$$

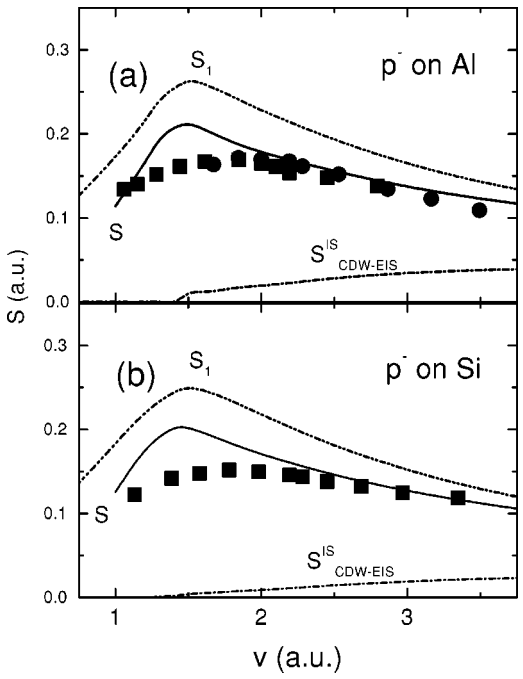

FIG. 4. Total stopping power for antiprotons on (a) aluminum and (b) silicon solid targets as a function of the impact velocity. Solid lines, total second-order stopping S as given by Eq. (19); double-dot–dashed lines, the total first-order stopping S_1 as given by Eq. (20); the dot-dashed lines, stopping due to the ionization of inner shells $2s$ and $2p$ calculated with the CDW-EIS approximation. The symbols represent the experiments for antiprotons (Ref. [23]).

The stopping S_{Born}^{IS} is calculated with the atomic first Born approximation, which is proportional to Z_P^2. S_{Born}^{IS} does not largely differ from $S_{CDW\text{-}EIS}^{IS}$ for the velocities of interest considered here. Furthermore, precisely in the region where the contributions are very different ($v \in \{1.4,2\}$ a.u.), inner-shell stopping can be neglected in comparison with S^{BC}. In this way, S_1 is a pure Z_P^2 contribution and the difference between S and S_1 gives essentially the information about the collisional contribution to order Z_P^3 due to binary encounters with both the FEG and the atomic electrons. Note that the full Z_P^3 correction to the stopping power should be obtained by including the second-order dielectric function in our calculation, employing the second-order P-e interaction developed by Pitarke *et al.* [21,22].

In Fig. 4 we plot the total stopping powers S and S_1 for $\bar{p}$ impinging on aluminum and silicon as a function of the impact velocity. As we are dealing with antiprotons, no structure effects are present. S values show a quite good agreement with experimental data [23] in the high-energy region. By comparing the results of S and S_1 we found that the Z_P^3 collisional correction is important even at the highest velocities studied. On the other hand, as any perturbative calculation, our theoretical results begin to fail for the lower velocities, i.e., $v \lesssim 2k_F$.

For incident hydrogen at intermediate energies, the different equilibrium state of charge of the exiting products must be included in the calculation of the stopping power. We

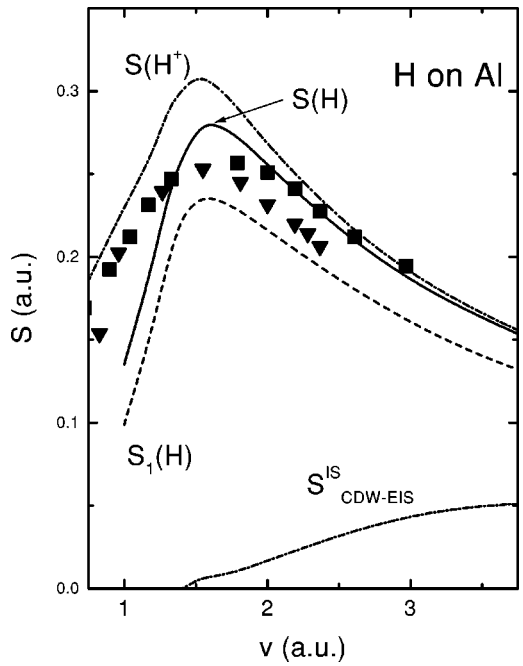

FIG. 5. Total stopping power for hydrogen on an aluminum solid target as a function of the impact velocity. Solid lines, total second-order stopping $S(H)$ as given by Eq. (21); dashed line, total first-order stopping $S_1(H)$; dot-dashed lines, partial second-order stopping power for H^+, $S(H^+)$. The symbols represent the experiments for hydrogen (Refs. [24–26]).

consider the outgoing projectiles H^+ and H^0 by weighting the corresponding fixed-charge stopping with the equilibrium fractions given by Peñalba *et al.* [8]. In the results of total stopping, we neglected the contributions of H^- and capture and loss processes, which have been estimated to be lower than 10% [8] for the velocities here considered. Therefore, the stopping of hydrogen is estimated as

$$S(H)=f^+S(H^+)+f^0S(H^0), \tag{21}$$

where the $f^{+,0}$ are the equilibrium charge state fractions of H^+ and H^0, respectively, and $S(H^{+,-})$ are the fixed charge partial stopping powers of H^+ and H^0, respectively [14]. Figure 5 shows the results that agree with experiments for high and medium velocities and start to depart in the low velocity regime.

To investigate the effect of the structure of the moving ion, $S(H^+)$ is also plotted in Fig. 5. The difference between $S(H)$ and $S(H^+)$ gives a measure of the influence of the structure. This difference is of the order of the Z_P^3 corrections at medium velocities and tends to zero at high impact velocities ($v>2k_F$), where Z_P^3 corrections are dominant.

IV. CONCLUSIONS

We calculate the second Born approximation of the stopping power within the BC formalism, conserving terms up to second order in the projectile charge. An induced wake potential expressed in terms of the Mermin-Linhard dielectric function is employed to describe the *P-e* interaction. Present calculations differ from the previous [3,4] in the fact that the potential considered here is reckoned as the full *cylindric*-induced potential. Z_P^3 collisional corrections to energy-loss distributions and stopping power are calculated for protons, neutral hydrogen, and antiprotons, considering the projectile charge as fixed. Up to second order, the BCF is found to properly describe the difference between protons and antiprotons stopping; protons deposit more energy in the high-energy tail, while, on the contrary, antiprotons diminish its contribution on such an energy region.

Using the Z_P^3 collisional term, the stopping of antiprotons in aluminum and silicon is calculated and compared with the first-order term, which depends on Z_P^2. Inner-shell stopping contributions are added using the CDW-EIS and first Born approximation, respectively. The agreement with the experiments is very good for $v\geqslant 2k_F$. We also inspect the case of protons moving in aluminum, taking into account the different equilibrium charge states of the projectile. Again for $v\geqslant 2k_F$ the theory predicts quite well a set of experiments.

ACKNOWLEDGMENTS

We would like to thank P. Echenique, J. Pitarke, and N. Arista for illuminating comments on the subject. This work was supported by CONICET and ANPCyT.

[1] D.G. Arbó and J.E. Miraglia, Phys. Rev. A **58**, 2970 (1998).
[2] P. Sigmund, Phys. Rev. A **26**, 2497 (1982).
[3] I. Nagy and P.M. Echenique, Phys. Rev. A **47**, 3050 (1993).
[4] I. Nagy and B. Apagyi, Phys. Rev. A **58**, R1653 (1998).
[5] H.H. Mikkelsen and P. Sigmund, Phys. Rev. A **40**, 101 (1989).
[6] D.S.F. Crothers and J.F. McCann, J. Phys. B **16**, 3229 (1983).
[7] N. Gulyas, P.D. Fainstein, and A. Salin, J. Phys. B **28**, 245 (1995).
[8] M. Peñalba, A. Arnau, P.M. Echenique, F. Flores, and R.H. Ritchie, Europhys. Lett. **19**, 45 (1992).
[9] J. Lindhard, K. Dan. Vidensk. Selsk. Mat. Fys. Medd. **28**, 8 (1954).
[10] N.D. Mermin, Phys. Rev. B **5**, 2362 (1970).
[11] P.M. Echenique, F. Flores, and R.H. Ritchie, Solid State Phys. **43**, 229 (1990), and references therein.
[12] For electron production calculations on surfaces see: F. García de Abajo, Nucl. Instrum. Methods Phys. Res. B **98**, 442 (1995); C.O. Reinhold and J. Burgdörfer, Phys. Rev. A **55**, 450 (1997).
[13] N.P. Wang and I. Nagy, Phys. Rev. A **55**, 2083 (1997).
[14] T. Kaneko, Phys. Rev. A **33**, 1602 (1986).
[15] R.A. Bonham and D.A. Kohl, J. Chem. Phys. **45**, 2471 (1976).
[16] N.R. Arista and A.F. Lifschitz, Phys. Rev. A **59**, 2719 (1999).

[17] I. Abril, R. Garcia-Molina, C.D. Denton, F.J. Pérez-Pérez, and N.R. Arista, Phys. Rev. A **58**, 357 (1998).
[18] P.D. Fainstein, V.H. Ponce, and R.D. Rivarola, J. Phys. B **24**, 3091 (1991).
[19] E. Clementi and C. Roetti, At. Data Nucl. Data Tables **14**, (1974).
[20] J. Oddershede and J. Sabin, At. Data Nucl. Data Tables **31**, 275 (1984).
[21] J.M. Pitarke, R.H. Ritchie, P. Echenique, and E. Zaremba, Europhys. Lett. **24**, 613 (1993).
[22] J.M. Pitarke, R.H. Ritchie, and P. Echenique, Phys. Rev. B **52**, 13 883 (1995).
[23] S.P. Møller *et al.*, Phys. Rev. A **6**, 2930 (1997).
[24] J.H. Ormrod and H.E. Duckworth, Can. J. Phys. **41**, 1424 (1963); J.H. Ormrod, J.R. MacDonald, and H.E. Duckworth, *ibid.* **43**, 275 (1965).
[25] W. White, J. Appl. Phys. **38**, 2660 (1967).
[26] S. Kreussler, C. Varelas, and R. Sizman, Phys. Rev. B **26**, 6099 (1982).